Geothermal Energy

RESEARCH Open Access

Exergy and exergoenvironmental assessment of a geothermal heat pump and a wind power turbine hybrid system in Shanghai, China

Yashar Aryanfar[1*] and Jorge Luis García Alcaraz[2]

*Correspondence:
yashar.aryanfar@gmail.com;
al216622@alumnos.uacj.mx

[1] Department of Electric Engineering and Computation., Autonomous University of Ciudad Juárez., Av. Del Charro 450 Norte. Col. Partido Romero., Juárez, Chihuahua, México
[2] Department Department of Industrial Engineering and Manufacturing, Autonomous University of Ciudad Juárez., Av. Del Charro 450 Norte. Col. Partido Romero., Juárez, Chihuahua, México

Abstract

Geothermal heat pumps are one of the most growing and cost-effective renewable energy technologies based on the temperature difference between the ground and the environment. In the cold seasons, the temperature inside the soil or water is higher than the ambient temperature. Therefore, the heat pump is used to extract the warm temperature of the ground into the house or any other controlled space. In the summer, the air temperature is higher than the temperature of the soil or water. This temperature difference is used again to cool the house or any other environment. This paper examines the energy and exergy assessments of a hybrid system in Shanghai, China, that employs a geothermal heat pump with an economizer for winter heating and a wind turbine to provide clean electricity. The complete set of procedures, as well as every component and every aspect of the hybrid system, have all been carefully examined. The heat pump's coefficient of performance is 3.916, its net power output is 22.03 kW, its overall energy efficiency is 77.2%, and its exergy efficiency is 25.49%.

Keywords: Heat pump, Geothermal, Wind turbine, Economizer, Shanghai

Graphical Abstract

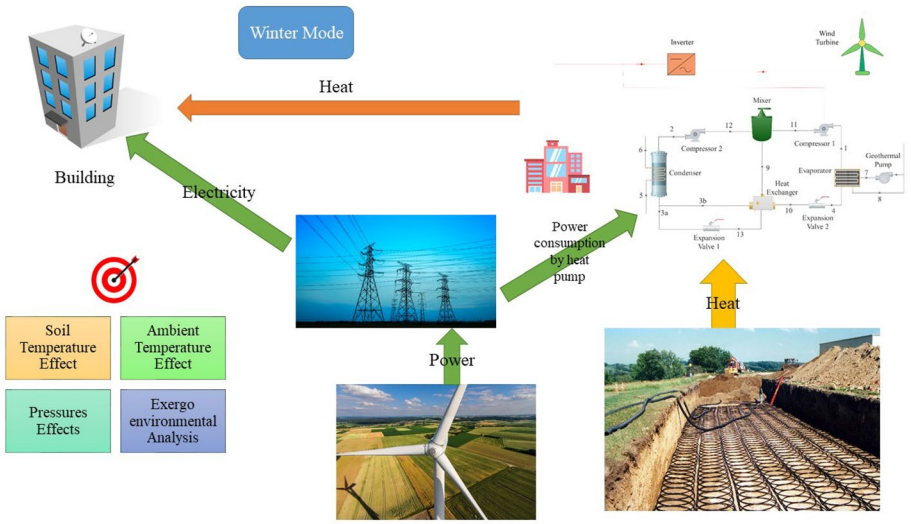

Introduction

Numerous issues have arisen for humankind because of his ever-increasing desire for energy and the rise in the use of fossil fuels. Among these difficulties are environmental concerns and the impending depletion of natural resources (Dolgun et al. 2023). The need for using clean and sustainable energies has been recognized because of these problems. As a result, using these kinds of resources for environmental issues became widely accepted (Gürbüz et al. 2022). These sources include novel energies, such as solar, wind, biomass, and others. The utilization of geothermal energy, or power drawn from the earth's interior, is another source that has long attracted attention (Lund et al. 2005). Numerous nations use this affordable, reliable, and pure energy source more frequently. The transformation of energy systems involves more than just increasing the use of renewable energy (Tang et al. 2022).

The use of heat pumps to electrify space heating is another essential component (Barton et al. 2013; Connolly 2017; Jacobson et al. 2017; Ruhnau et al. 2019). Decarbonization goals are anticipated to accelerate this trend, because electric heating produced with renewable energy has a lower carbon footprint than fossil fuel alternatives. Like power generation from fluctuating renewable sources, decentralized heat pumps' electricity consumption is inherently unstable; it depends on the heat demand and heat pump efficiency, which change over time because of the surrounding environment and human activities. These oscillations, which exhibit both predictable (diurnal, seasonal) and random (weather-related) patterns, are like renewable production sources in that they could provide extra difficulties for the energy system. For instance, earlier research has shown that heat pumps increase the peak load on electrical systems, necessitating more dispatchable backup generation capacity (Baeten et al. 2017; Bloess et al. 2018; Cooper et al. 2016; Fehrenbach et al. 2014; Hedegaard

and Münster 2013; Patteeuw et al. 2015; Quiggin and Buswell 2016; Waite and Modi 2020; Wilson et al. 2013). Through electrical systems and markets, renewables and heat pumps interact in three ways: heat pumps raise the demand for renewable power, heat demand and renewable supply is correlated over time, and heat pumps may offer flexibility to the electricity system. Heat pumps, which are, in fact, a particular kind of demand response, can give the electrical grid flexibility. They can shift their electricity consumption to periods of low pricing and abundant renewable energy by adopting thermal storage (Fuzhang et al. 2021; Kandiri et al. 2022; Wang et al. 2022). Such a flexible functioning of heat pumps can further reduce wind power curtailment compared to an inflexible operation, which ignores electricity pricing and renewable supplies. However, even with a flexible process, heat pumps improve the peak capacity of the electrical system compared to not using them at all (Arteconi et al. 2016; Nazar et al. 2022).

The conceptualization and techno-economic–environmental analysis of an innovative power-to-heat system based on the excess energy from solar photovoltaic (PV) plants and open-loop geothermal heat pumps (GHPs) were investigated by Allouhi (2022). Numerous scenarios were looked through, and corresponding ideal designs were found. The ideal PV capacity to be installed is 26 kWp when considering the annual electric and heat demand of 207.46 MWh_{ele} and 13.67 MWh_{th} in the residential neighborhood and the primary school, respectively. Based on the load characteristics of a shelter underneath the streets of Beijing, China, Zeng et al. (2022) investigated the thermo-economic performance of the hybrid system in the two modes. The impact of pipe length, multi-modular water-PCM tank matrix, and cooling water flow ratio on the energy and economic performance of the components are investigated and optimized using the Taguchi design approach. The outcome demonstrates that, when operating for 10 years, 75% of the base ground heat exchangers (GHE) could ensure that the cooling water temperature would remain within a specific range in normal mode. Experimental and numerical research was conducted by Rodriguez-Alejandro et al. (2022) on a vertical ground-source heat pump operating as an air conditioner. The geothermal heat pump, which has a depth of 100 m and a volume of 41.16 m^3, is situated in Mexico. To analyze the system's thermal performance in the weather conditions of Mexico and to determine the cost allocation per piece of equipment in the system, a computational fluid dynamics study of the geothermal heat exchanger and a thermoeconomic analysis of the heat pump are constructed. According to the findings, a geothermal heat pump offers a comfortable temperature and the lowest comfort relative humidity.

This article studies the energy and exergy analyses of a hybrid system that uses a geothermal heat pump equipped with an economizer for winter heating and a wind turbine for environmentally friendly power generation in Shanghai, China. The hybrid system's entire set of processes, as well as all its parts and the whole system, have all been thoroughly explored. The innovation of the present work is to propose and then analyze the energy and exergy of a hybrid system that includes a geothermal heat pump coupled with a wind turbine to supply the heat and power needed for a residential unit in winter for the city of Shanghai in China. So far, only a few studies have been done on combined heat pump–wind turbine systems, and the research gap in this matter is noticeable. The following are the study's broad goals:

- Designing and simulation of a new hybrid heat and power generation system including a geothermal heat pump and a wind turbine.
- Investigating the effect of changes condenser pressure, evaporator pressure, intermediate pressure, ambient temperature and soil temperature on the energy and exergy efficiencies, COP of the heat pump and the system's net power output
- Calculation of exergy destruction of different system components
- Exergeoenvironmental analysis of the proposed heat pump system

In the present work, first the proposed hybrid system is explained and the equations governing the different parts of the system are presented. The modeling process is carried out in the EES software environment, and the output results are validated with previous studies. Next, the system is studied from the point of view of Moore's energy and exergy, and the effects of changes in system input parameters on the design parameters are studied.

Modeling and cycle description

Figure 1 shows a combined system, including a geothermal heat pump with an intermediate economizer and a wind turbine. By producing power, the wind turbine, in addition to meeting the demand of the geothermal heat pump, will also provide the electricity consumed by the residential unit, and the rest of the generated electricity will be injected into the grid. The geothermal evaporator (point 1) heats the refrigerant (R134a) before it enters the evaporator at point 4, which produces hot steam. After exiting the evaporator, the refrigerant enters the compressor, increasing the pressure in the superheated mode at medium pressure. To mark the cycle's conclusion, the output currents from compressor 1 and the heat exchanger are blended in the mixer at point 11. According to Ma and Chai (2004), the thermodynamic conditions at points 9 and 11 must be the same for the mixer's output current and the intake to compressor 2 (point 12) to be saturated or

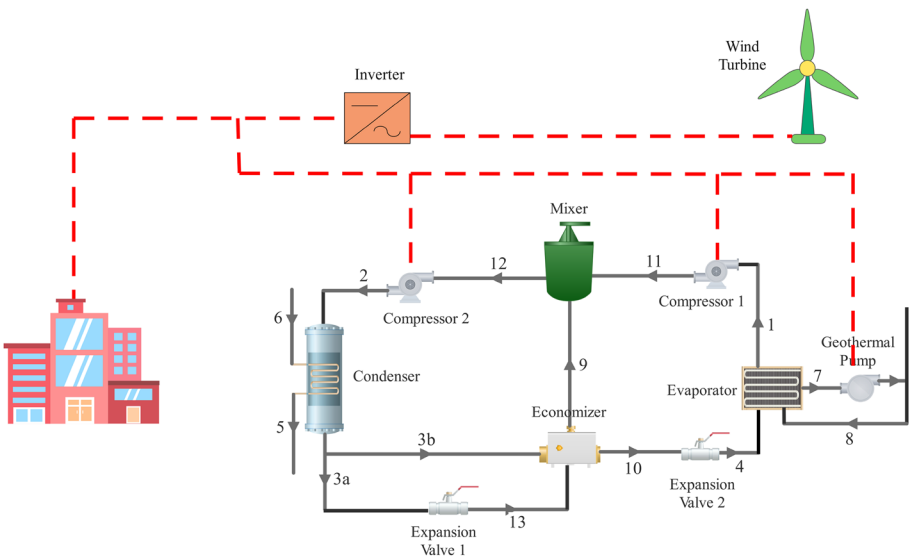

Fig. 1 Schematic of geothermal heat pump and wind turbine hybrid system

superheated. After receiving the mixer's output current, compressor 2 increases pressure until it reaches point 2, the cycle's top condenser, where it distributes heat to heat the ventilated room. The condenser output current is divided into two halves and is the refrigerant (point 3). The remaining fluid enters the heat exchanger (main current). It heats the intake to the mixer and the outlet of the pressure expansion valve 1 by raising the temperature below the refrigerant at the exit (point 10) (Self et al. 2012). A portion of the fluid flows to the pressure expansion valve 1, which lowers the pressure using a constant enthalpy process until it reaches the cycle's middle pressure (point 13). The fluid from the heat exchanger (point 10) ultimately passes the pressure expansion valve 2 and enters the evaporator after reaching the cycle's lower pressure.

The thermodynamic analysis of the ground source heat pump system from the perspective of performance coefficient and exergy efficiency is performed using the first and second laws of thermodynamics for different components of the cycle and using organic fluid R134a, which is a standard fluid for the steam compression cycle. The analysis of the first law examines the quantity of energy exchange, and the study of the second law examines the quality of energy exchange. Irreversibility in different components of a thermodynamic cycle causes system performance to decline. In an actual process, some external or internal factors cause entropy production. Internal entropy production in the heat pump cycle mainly occurs from pressure drop in the pipes and internal heat transfer due to the specific temperature difference in the system components. In addition, the production of external entropy occurs due to heat transfer outside the boundaries of the control volume.

The wind profile over the rotor-swept region is defined to examine wind turbine performance using the Rankine–Froude Actuator disc theory (Esposito 1998; Johnson 1985; Khalil 2007). Additional hypotheses are considered in the system modeling, including:

(1) The soil below the surface is uniform.
(2) Throughout the investigated temperature range, the thermal characteristics of every material remain constant.
(3) Contact resistance exists between the ground and the boreholes.
(4) The ground's temperature is constant above and far below the boreholes.
(5) The soil's ability to conduct heat vertically needs to be considered.
(6) The system works in stable mode.
(7) The pressure drops in heat exchangers and connecting pipes are negligible.
(8) The isentropic efficiency of the compressors is 0.8, and the isentropic efficiency of the pump is 0.9.
(9) The geothermal fluid is a mixture of water and ethanol with a mass percentage of 30% ethanol in water.
(10) The wind flow is assumed to be homogeneous and incompressible.
(11) The flow velocity in the disc is assumed to be uniform.
(12) There are no obstructions to wind flow upstream or downstream of the rotor.
(13) The wind flow passing through the disk is non-rotating.

Figure 2 also shows the temperature–entropy diagram of the heat pump section. The working principle of a heat pump is based on a physical property, which increases the

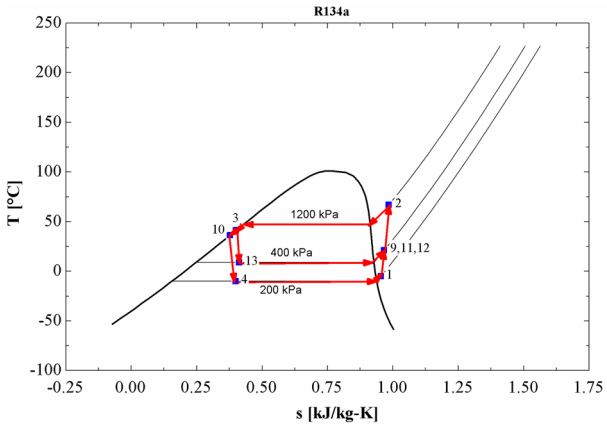

Fig. 2 T–s diagram for the heat pump

boiling point of a fluid with increasing pressure. By reducing the pressure, the refrigerant can vaporize at low temperatures, while increasing the pressure will increase its boiling point. The heat pump or heat pump system is a refrigeration cycle that can transfer heat to the desired direction through a particular control. This way, the evaporator and condenser of this refrigeration cycle will alternately play each other's roles depending on the season. This system is affordable for countries, where electricity is cheaper than fossil fuels and has a unique appeal. All air conditioning systems can be converted into heat pump or heat pump systems.

Governing equations

Heat pump section

With constant flow conditions and the assumption of each cycle component as the control volume, the energy balance and the irreversibility equations in each of the components are written as the following (Hepbasli 2005; Huang et al. 2023):

$$\dot{Q} - \dot{W} + \sum \dot{m}_{in} h_{in} + \sum \dot{m}_{out} h_{out} = 0 \tag{1}$$

$$\dot{I} = \dot{m} T_0 \frac{ds_{total}}{dt} \tag{2}$$

In Eq. 1, $\dot{Q}$, $\dot{W}$, $\dot{m}$ and h are the rate of heat exchanged, work exchanged, mass flow rate and specific enthalpy, respectively, the subscripts *in* and *out* are related to the input flows to the control volume, and the output flows from the control volume, respectively. In Eq. 2, $\dot{I}$, T_0, and s are irreversibility, ambient temperature, and specific entropy, respectively. Equation 2 is expanded as follows (Ural et al. 2021):

$$\dot{I} = \dot{m} T_0 \left(\sum s_{out} - \sum s_{in} + \frac{ds_{system}}{dt} + \sum \frac{q_k}{T_k} \right) \tag{3}$$

In Eq. 3, T_k is the temperature of the heat source, and q_k is the amount of heat transfer per unit of mass between the heat source and the working fluid; if the system reaches a steady state, it becomes $\frac{ds_{system}}{dt} = 0$.

The internal irreversibilities in the system components are calculated using the $\sum s$ term, and the external irreversibilities are calculated using the $\sum \frac{q}{T}$ term. In addition, in this research, internal irreversibilities corresponding to pressure drops in system components such as heat exchangers and pipes are omitted for simplicity. The above equations are written separately for each cycle component to obtain work, heat exchange, and irreversibility. In addition, to obtain exergy efficiency and exergy destruction fraction in different components of the cycle, Eqs. 4 and 5 are used (Hepbasli 2005):

$$\eta_{ex,i} = \frac{\dot{E}x_{desired,out}}{\dot{E}x_{used}} \tag{4}$$

$$y_{ex,i} = \frac{\dot{I}_i}{\dot{I}_{tot}} \tag{5}$$

In Eq. 4, η_{ex} is the exergy efficiency, $\dot{E}x_{desired,out}$ is the exergy corresponding to the desired output currents, and $\dot{E}x_{used}$ is the exergy corresponding to the input supply currents, and in Eq. 5, y_{ex} is the exergy destruction fraction (Self et al. 2013). To obtain the flow rate of different parts of the cycle, the laws of conservation of mass and energy result in the following equations (Self et al. 2013):

$$\dot{\mathrm{m}}_{\mathrm{ref}} = \frac{\dot{\mathrm{Q}}_{\mathrm{cond}}}{\mathrm{h}_2 - \mathrm{h}_3} \tag{6}$$

$$\dot{\mathrm{m}}_{\mathrm{sup}} = \dot{m}_{ref} \frac{h_{10} - h_3}{\mathrm{h}_{13} + h_{10} - \mathrm{h}_3 - h_9} \tag{7}$$

$$\dot{\mathrm{m}}_{\mathrm{main}} = \dot{\mathrm{m}}_{\mathrm{ref}} \frac{\mathrm{h}_9 - \mathrm{h}_{13}}{\mathrm{h}_3 + \mathrm{h}_9 - \mathrm{h}_{13} - \mathrm{h}_{10}} \tag{8}$$

Which $\dot{m}_{ref}$, $\dot{m}_{sup}$ and $\dot{m}_{main}$ are mass flow rates through the condenser, expansion valve 1, and evaporator, respectively (Self et al. 2013), and $\dot{Q}_{cond}$ is the rate of heat exchanged in the condenser.

$$\dot{\mathrm{Q}}_{\mathrm{Cond}} = \dot{\mathrm{m}}_2 \mathrm{h}_2 - \dot{\mathrm{m}}_2 \mathrm{h}_3 \tag{9}$$

In the present study, the system capacity is assumed to be 100 kW ($\dot{Q}_{cond} = 100kW$). The work of the geothermal pump is obtained from the following equation (Sayyaadi et al. 2009):

$$\dot{\mathrm{w}}_{\mathrm{pump,gl}} = \frac{\dot{\mathrm{V}}_{w,gl} \Delta \mathrm{P}_{w,gl}}{\eta_{\mathrm{pump}}} \tag{10}$$

where $\dot{V}_{w,gl}$ is the volume flow rate of the fluid in the geothermal ring, η_{pump} is the isentropic efficiency of the pump, and $\Delta \mathrm{P}_{w,gl}$ is the pressure drop of the fluid in the geothermal ring, which is obtained from the following equations:

$$\Delta P_{w,gl} = f * \left(\frac{l_{gl} \rho_{w,gl} V_{w,gl}}{2 d_{i,gl}} \right) \tag{11}$$

$$f = (0.79 ln Re_{w,gl} - 1.64)^{-2} \tag{12}$$

In the above relationships, $\rho_{w,gl}$ is the fluid density, $V_{w,gl}$ is the fluid velocity, and $Re_{w,gl}$ is the Reynolds number of the fluid inside the geothermal exchanger, as well as $d_{i,gl}$ and l_{gl}, respectively, are the internal diameter and length of the geothermal tube, and the length of the geothermal tube is calculated through Eq. 13:

$$l_{gl} = \frac{\left(\frac{\dot{Q}_{eva}}{N_b} \right)}{T_s - T_{w,gl}} \cdot \left(\frac{1}{\pi d_{i,gl} h_{w,gl}} + \frac{\ln(\frac{d_{o,gl}}{d_{i,gl}})}{2 k_{gl}} + \frac{F}{U_s d_{o,gl}} \right) \tag{13}$$

In Eq. 13, $T_{w,gl}$ is the average temperature of the fluid inside the geothermal tube, N_b and $d_{o,gl}$ are the number and outer diameter of U-shaped geothermal tubes placed in parallel, $h_{w,gl}$ is the heat transfer of the fluid displacement inside the geothermal tube, k_{gl} is the heat transfer coefficient of the tube. F is the ratio of the number of hours of maximum load to the total number of hours required for heating in the ventilated space. In addition, T_s and U_s are soil temperature and soil heat transfer coefficient, respectively, and $\dot{Q}_{eva}$ is the rate of heat exchanged in the evaporator. Finally, the coefficient of performance (COP) and exergy efficiency of the heat pump and the whole system are obtained from Eqs. 14, 15, 16 and 17 (Esen et al. 2007):

$$COP_{hp} = \frac{\dot{Q}_{cond}}{\dot{W}_{comp1} + \dot{W}_{comp2}} \tag{14}$$

$$\dot{W}_{net} = q(v) - \dot{W}_{comp1} - \dot{W}_{comp2} - \dot{W}_{pump,gl} \tag{15}$$

$$\eta_{en,tot} = \frac{\dot{Q}_{cond} + \dot{W}_{net}}{\dot{Q}_{geo,in} + \dot{W}_{wind}} \tag{16}$$

$$\eta_{ex,tot} = \frac{\dot{E}x_{cond} + \dot{W}_{net}}{\dot{E}x_{in,gl} + \dot{W}_{wind}} \tag{17}$$

The works of compressor 1 and compressor 2 is obtained from Eqs. 18 and 19:

$$\dot{W}_{comp1} = \dot{m}_{main}(h_{11} - h_1) \tag{18}$$

$$\dot{W}_{comp2} = \dot{m}_{ref}(h_2 - h_{12}) \tag{19}$$

Wind turbine section

Using the power curves provided by the manufacturer, technical specifications are usually extracted based on the fundamental equation, independent of temperature,

pressure, humidity, and air density. In this way, the curves introduced by the manufacturer do not conform to the actual conditions in which the turbine is installed. Therefore, power plants need to model the power curve based on real conditions to control the output power of the turbines. In the parametric approach, the types of curves that are used to model the nonlinear part of the power curve are:

- Quadratic polynomial power curve
- Exponential curve
- Cube power curve
- Approximate cubic power curve

In the quadratic polynomial power curve, the power in terms of speed is approximated by a second order polynomial in the form of the following equation (Ouyang et al. 2017):

$$q(v) = C_1 + C_2 v + C_3 v^2 \tag{20}$$

So that C_1, C_2 and C_3 are constants that are obtained based on the information of v_{ci}, v_r and P_r, respectively, using the following equations:

$$C_1 = \frac{1}{(v_{ci} - v_r)^2}\left[v_{ci}(v_{ci} + v_r) - 4v_{ci}v_r\left(\frac{v_{ci} + v_r}{2v_r}\right)^3\right] \tag{21}$$

$$C_2 = \frac{1}{(v_{ci} - v_r)^2}\left[4(v_{ci} + v_r)\left(\frac{v_{ci} + v_r}{2v_r}\right)^3 - 4v_{ci}v_r\left(\frac{v_{ci} + v_r}{2v_r}\right)^3 - 3v_{ci} - v_r\right] \tag{22}$$

$$C_3 = \frac{1}{(v_{ci} - v_r)^2}\left[2 - 4\left(\frac{v_{ci} + v_r}{2v_r}\right)^3\right] \tag{23}$$

When the exponential power curve in a variable speed wind turbine is used to model the power curve, the nonlinear part of the power curve is approximated as the following equation (Mathew 2006):

$$q(v) = \frac{1}{2}\rho A K_p (v^\beta - {v_{ci}}^\beta) \tag{24}$$

where A equals the area swept by the blades, ρ equals the air density of the area, v_{ci} equals the cut-in speed, and K_p and β are constant values. The cubic power curve is obtained by simplifying Eq. (25), so that β is equal to 3 and v_{ci} is assumed to be zero. In this case, the power curve is simplified as Eq. (25) (Thiringer and Linders 1993):

$$q(v) = \frac{1}{2}\rho A C_{p,eq} v^3 \tag{25}$$

where $C_{p,eq}$ is the constant of the cubic coefficient, which is equivalent to the power factor. The approximate cubic power curve is an approximation of Eq. (26), where $C_{p,eq}$ is approximated by its maximum value, which is denoted by $C_{p,max}$; Therefore, the nonlinear part of the power curve is shown according to Eq. (27) (El-Shimy 2010):

$$q(v) = \frac{1}{2}\rho A C_{p,max} v^3 \tag{26}$$

$$q(v) = C_{p,max} \dot{W}_{wind} \tag{27}$$

Exergoenvironmental analysis section

Exergoenvironmental analysis is used to assess system performance from an environmental point of view. The analyses' guiding principles are formed based on evaluations of the thermodynamic and ambient conditions. The following is how the exergoenvironment factor can be expressed (Ahmadi et al. 2020):

$$f_{ei} = \frac{\dot{E}x_{tot.des}}{\sum \dot{E}x_{in}} \tag{28}$$

Subscripts *in* and *tot.des* stand for system input and total exergy destruction, respectively, while $\dot{E}x$ is the exergy rate. The exergy stability factor can be determined using Eq. 29 (Ahmadi et al. 2020):

$$f_{es} = \frac{\dot{E}x_{tot.des}}{\dot{E}x_{tot.out} + \dot{E}x_{tot.des} + 1} \tag{29}$$

where the subscript *tot.out* denotes the system's total energy destruction. As a result, the total exergy destruction rate is directly correlated with the exergoenvironment and exergy stability factors. The following equation yields the exergoenvironmental effect coefficient (Ahmadi et al. 2020):

$$C_{ei} = {}^{1}/_{\eta_{ex}} \tag{30}$$

where η_{ex} denotes the system's exergy efficiency. The following equation is how the efficacy factor for environmental damage is calculated (Ahmadi et al. 2020):

$$\theta_{ei} = f_{ei}.C_{ei} \tag{31}$$

However, the impact of exergoenviornmental enhancement can be estimated as(Ahmadi et al. 2020):

$$\theta_{eii} = \frac{1}{\theta_{ei}} \tag{32}$$

Figure 3 presents the solution flowchart of the proposed system. Algorithms are written to solve problems. The most challenging part of solving the problem is designing its algorithm. In developing the algorithm, first, determine the general steps of doing the work, and by solving each primary stage, the whole problem is solved. Algorithms often have the following steps:

1. Read data
2. Perform calculations
3. Print the results

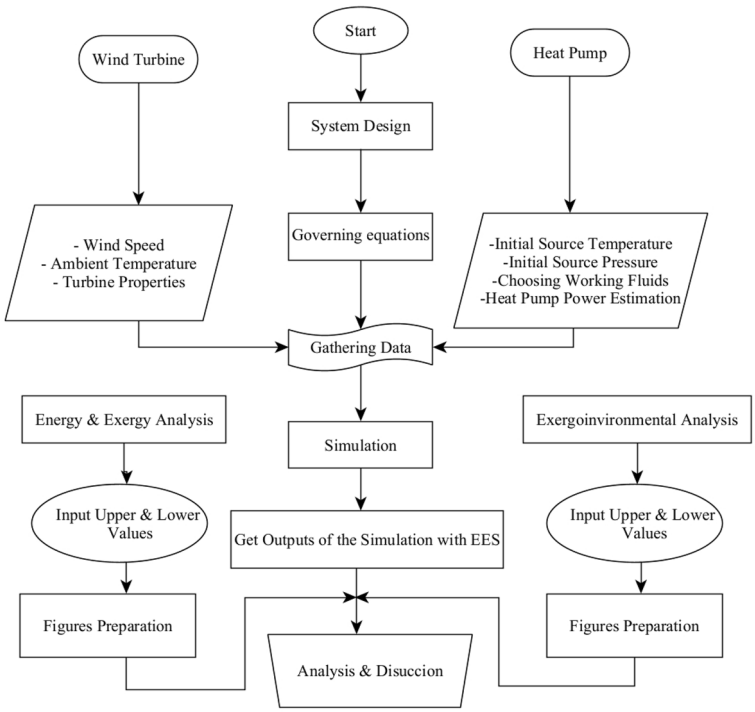

Fig. 3 Process flowchart for solving problems

With careful consideration, each step of the algorithm may be divided into smaller parts. For example, performing calculations is a general stage that, by addressing the problem, turns into mathematical relationships that solve the problem. In principle, to solve a problem and design an algorithm for it, the following must be specified:

- A precise definition of the problem to determine its requirements
- Problem inputs
- Outputs of the problem
- Examining different solutions to the problem
- The relationship between the inputs and outputs of the problem
- Choosing a suitable solution and preparing an algorithm for that solution
- Algorithm debugger

Working fluid and initial condition

R134a has been selected as the investigation's working fluid. The working fluid's parameters are shown in Table 1. Standard Boiling Point, Critical Temperature, and Critical Pressure are three of the most important factors influencing fluid choice. The table below includes each refrigerant gas' chemical name and formula, which were taken from the ANSI/ASHRAE standard 34-2010 for refrigerant gases (refrigerant compressor gas). Table 2 provides a list of the main input variables for the simulation of the current heat pump.

Table 1 Properties of the refrigerant (Ata et al. 2020; Devecioğlu and Oruç 2017)

Refrigerant	Molecular formula	Molecular weight [kg/kmol]	Normal boiling point (°C)	Critical temperature (°C)	Critical pressure (MPa)	Safety class	ODP	GWP
R134a	CH2FCF3	102	−26.4	101.1	4.059	A1	0	1430

Table 2 Initial conditions for Shanghai city in winter

Sign	Definition	Amount	References
P_0[kPa]	Ambient pressure	101.2	–
T_0[°C]	Ambient temperature	6	(Huang et al. 2021)
P_1[kPa]	Evaporator pressure	200	(Pishkariahmadabad et al. 2021)
P_2[kPa]	Condenser pressure	400	(Pishkariahmadabad et al. 2021)
P_9[kPa]	Heat exchanger temperature	1200	(Pishkariahmadabad et al. 2021)
T_{soil}[°C]	Soil temperature	15	(Zhai and Yang 2011)
η_{comp1}	Compressor 1 efficiency	0.8	(Pishkariahmadabad et al. 2021)
η_{comp2}	Compressor 2 efficiency	0.8	(Pishkariahmadabad et al. 2021)
$\eta_{geopump}$	Geothermal pump efficiency	0.9	(Pishkariahmadabad et al. 2021)
T_5[°C]	Heated water temperature	35	(Pishkariahmadabad et al. 2021)
T_6[°C]	Entrance water temperature	30	(Pishkariahmadabad et al. 2021)
T_7[°C]	Geothermal pump entrance temperature	7	(Pishkariahmadabad et al. 2021)
T_8[°C]	Geothermal pump exit temperature	11	(Pishkariahmadabad et al. 2021)
$\dot{Q}cond$[kW]	Condenser capacity	100	(Pishkariahmadabad et al. 2021)
$U_s[\frac{W}{m^2k}]$	Soil heat transfer coefficient	12	(Sanaye and Niroomand 2009)
F	The ratio of the number of hours of maximum load to the total number of hours	0.4	(Sanaye and Niroomand 2009)
$k_{gl}[\frac{W}{mk}]$	Heat transfer coefficient of the tube	0.45	(Sayyaadi et al. 2009)
d_i[m]	Internal diameter	0.0218	(Sayyaadi et al. 2009)
d_o[m]	Outer diameter	0.0267	(Sayyaadi et al. 2009)
$V[\frac{m}{s}]$	Fluid speed inside the geothermal tube	1	(Sayyaadi et al. 2009)

Figure 4 shows the aerial view of Shanghai, China. This image is taken from RetScreen software. Shanghai is one of the largest cities in China and the second largest city in the world after Tokyo, which is China's economic and most populous capital. China is the world's largest and most polluting country in terms of production and use of clean energy. However, the growth rate of renewable energy consumption in China is faster than of fossil fuel consumption. The share of renewable energy production in the country's total energy production is about 28%, which is higher than the average production in Europe. If the current trend continues, this share is expected to be at the world's top in a decade.

Figure 5a, b shows the minimum and maximum temperatures for different months in Shanghai, China. These outputs are taken from Meteonorm software, and Table 3 shows the characteristics and input data of the wind turbine.

Results and discussion

Using the heat pump mechanism, you can prepare hot water, cold water, or hot and cold air, depending on the season, with a refrigeration machine without needing a boiler. The use of this system reduces the initial cost of the installation and the space

Fig. 4 Shanghai city location

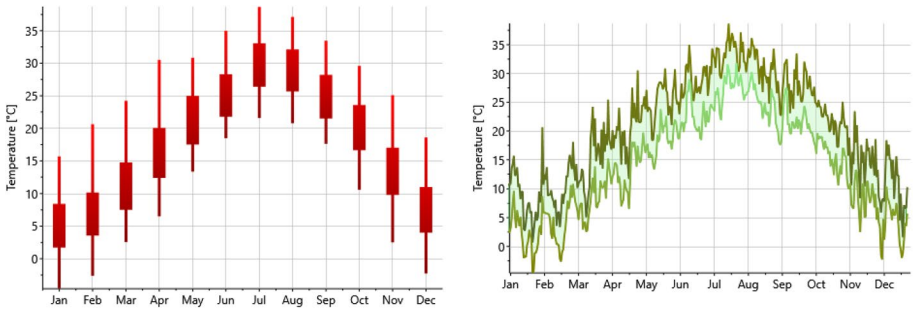

Fig. 5 Shanghai city temperature during the year

Table 3 Wind turbine features

Sign	Definition	Amount	References
D[m]	Turbine diameter	34	–
V[m/s]	Wind speed in Shanghai	5.5	(Huang et al. 2021)
η_{wt}[-]	Wind turbine efficiency	0.9	(Pishkariahmadabad et al. 2021)
C_{pwt}[-]	Max efficiency	0.59	(Pishkariahmadabad et al. 2021)
ρ_{air}[kg/m^3]	Density of air	1.23	(Pishkariahmadabad et al. 2021)

required in the engine room. In addition, reducing fossil fuel consumption reduces air pollution and increases building safety in the face of risks, such as fire, etc.

EES software simulated all equations for mass and energy conservation in parts and irreversibility relations in various parts of the heat pump cycle. This software provides a subset of several fluid parameters that can be used to model the cycle (in this case, using R134a fluid). To study the parameter in the fundamental working mode, the cycle's high, middle, and low pressures are taken as 1200, 400, and 200 kPa, respectively. It is anticipated that there will be a 5 °C difference between the output of the condenser and evaporator. The simulation results are shown in Table 4, along with values for mass flow rate, pressure, temperature, enthalpy, and entropy at various system sites.

To corroborate the findings, the effects of high-pressure changes on the heat pump's coefficient of performance with identical input cases have been compared with those of Self et al. The standard deviation of the results is acceptable. Figure 6 shows the validation of the present work.

Table 5 displays the modeling results for the system under investigation. Based on Table 5, an estimate of the heat pump's COP and overall system energy efficiency is made. Environmental parameters are also calculated and reported in the table, including the Exergoenvironment factor, Exergy stability factor, Exergoenvironmental impact coefficient, Environmental damage effectiveness factor, and Exergoenvironmental impact improvement factor. According to Table 3, the total turbine production power is equal to 49.33 kW according to the wind turbine's specifications and the average wind speed in Shanghai. This production power provides the heat pump components, and the rest is transferred to the network.

Table 4 Properties of system's different points

State	Working fluid	Mass flow rate (kg/s)	Pressure (kPa)	Temperature (°C)	Enthalpy (kJ/kg)	Entropy (kJ/kg)
1	R134a	0.5101	200	−5.093	248.7	0.9538
2	R134a	0.5343	1200	66.99	297.3	0.9843
3	R134a	0.5343	1200	41.29	110.2	0.4004
4	R134a	0.5101	200	−10.09	102.7	0.399
5	water	4.782	250	35	146.8	0.5049
6	water	4.782	250	30	125.9	0.4365
7	Geo-fluid	4.432	250	7	28.47	–
8	Geo-fluid	4.432	250	11	45.27	–
9	R134a	0.02421	400	21.1	266.9	0.9662
10	R134a	0.5101	1200	36.29	102.7	0.3766
11	R134a	0.5101	400	21.1	266.9	0.9662
12	R134a	0.5343	400	21.1	266.9	0.9662
13	R134a	0.02421	400	8.91	110.2	0.4115

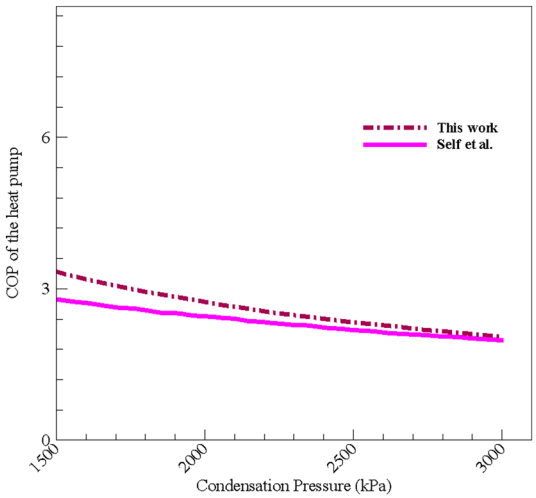

Fig. 6 Comparison of the results of the present work with the results of Self et al. (Self et al. 2013, 2012) (The effect of condensation pressure changes on the heat pump coefficient of performance)

Figure 7a shows the effects of condenser pressure changes on energy efficiency and exergy efficiency. By increasing the condenser pressure from about 1050 to 1550 kPa, the energy efficiency of the proposed system decreases from 77.5 to 76.5%. In the case of exergy efficiency, it drops from 25.85 to 24.85%. Therefore, increasing the condenser pressure will harm the system's efficiency. The reason for this will be the increase in the work of the compressors.

Figure 7b also shows the effects of condenser pressure changes on the net power output and coefficient of performance (COP) of the heat pump. By increasing the condenser pressure from about 1050 to 1550 kPa, the net power output of the proposed system is reduced from 24.5 to 17.5 kW. In the case of coefficient of performance of the heat pump, it is reduced from 4.3 to 3.2. Therefore, increasing the condenser

Table 5 System output results

Parameters	Definition	Value
$\dot{m}_{sup}$ (kg/s)	The mass flow rate through expansion valve 1	0.02421
$\dot{m}_{main}$ (kg/s)	The mass flow rate through the evaporator	0.5101
$\dot{W}_{comp1}$ (kW)	Compressor 1 work	9.26
$\dot{W}_{comp2}$ (kW)	Compressor 2 work	16.28
COP_{hp}	Performance coefficient of heat pump	3.916
$\dot{W}_{net}$(kW)	Wind turbine work	49.33
$\dot{W}_{net}$(kW)	Net power output	22.03
$\eta_{en,total}$	The exergy efficiency of the total system	77.2%
$\eta_{ex,total}$	The exergy efficiency of the total system	25.49%
f_{ei}	Exergoenvironment factor	0.9704
f_{es}	Exergy stability factor	0.56
C_{ei}	Exergoenvironmental impact coefficient	3.923
θ_{ei}	Environmental damage effectiveness factor	3.806
θ_{eii}	Exergoenvironmental impact improvement factor	0.2627

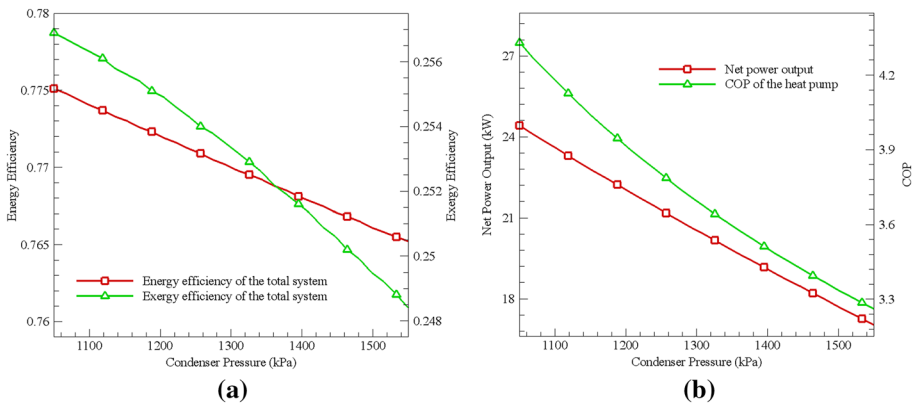

Fig. 7 Effect of condenser pressure changes on **a** energy efficiency and exergy efficiency, **b** net power output and coefficient of performance of the heat pump

pressure harms these two performance parameters of the system. As mentioned, the reason for this will be the increase in the work of the compressors.

Figure 8a shows the effects of evaporator pressure changes on energy efficiency and exergy efficiency. By increasing the condenser pressure from 153 to 300 kPa, the energy efficiency of the proposed system rises from 76.76 to 77.86%. In the case of exergy efficiency, it rises from 24.4 to 27.21%. Therefore, increasing the condenser pressure will have a positive effect on the efficiency of the system. The reason for this will be the reduction of compressors. Figure 8b also shows the impact of evaporator pressure changes on the total output work and heat pump performance coefficient. By increasing the condenser pressure from 153 to 300 kPa, the net power output of the proposed system increases from 18.8 to 27.18 kW. Regarding the heat pump performance factor, it increases from 3.466 to 4.935. Therefore, increasing the condenser pressure positively affects these two performance parameters of the system. As mentioned, the reason for this will also be the reduction of the work of the compressors.

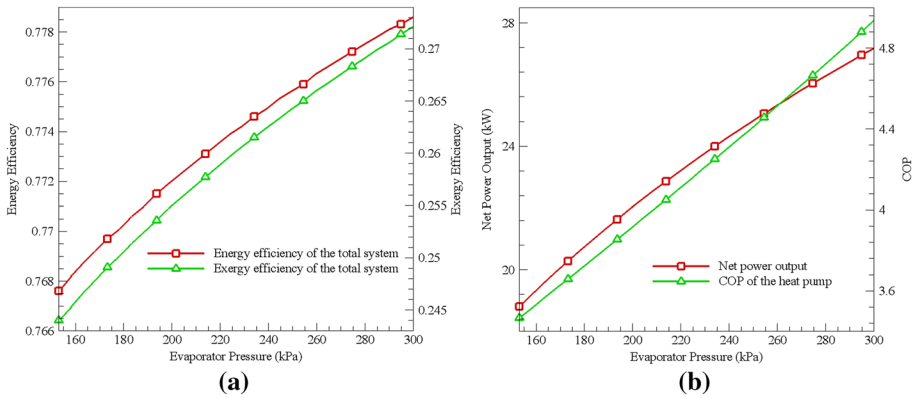

Fig. 8 Effect of evaporator pressure changes on **a** energy efficiency and exergy efficiency, **b** net power output and coefficient of performance of the heat pump

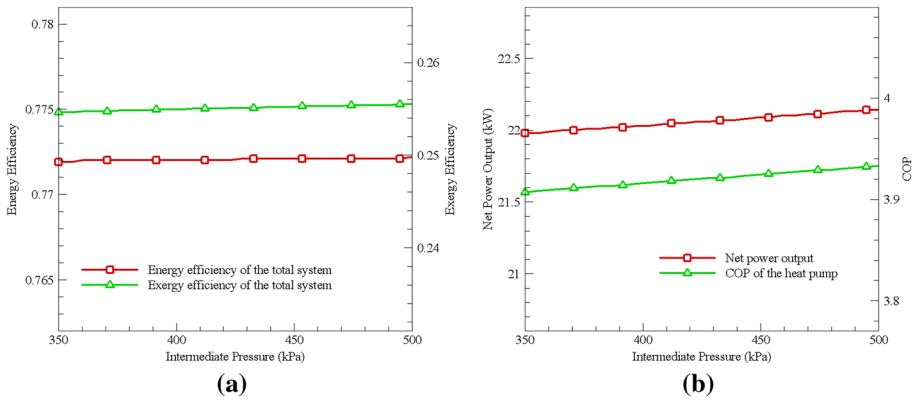

Fig. 9 Effect of intermediate pressure changes on **a** energy efficiency and exergy efficiency, **b** net power output and coefficient of performance of the heat pump

Figure 9a shows the effects of system intermediate pressure changes on energy and exergy efficiency. By increasing the condenser pressure from 350 to 500 kPa, the energy efficiency of the proposed system increases from 77.19 to 77.22%. In the case of exergy efficiency, it rises from 25.46 to 25.55%. Therefore, increasing the condenser pressure will have a positive effect on the efficiency of the system. The reason for this will be the reduction of compressors. Figure 9b also shows the impact of changes in the medium pressure of the system on the total output work and the coefficient of performance of the heat pump. By increasing the condenser pressure from 350 to 500 kPa, the net power output of the proposed system increases from 21.98 to 22.14 kW. In the case of the heat pump coefficient of performance, it rises from 3.907 to 3.933. Therefore, increasing the condenser pressure positively affects these two performance parameters of the system. As mentioned, the reason for this will also be the reduction of the work of the compressors. Of course, the effect of changes in the mean pressure on these four parameters is minimal.

Figure 10a shows the effects of ambient temperature changes on energy efficiency and exergy efficiency. As the ambient temperature increases from 1 to 11 °C, the system's energy efficiency remains constant at 77.2%. However, in the case of exergy

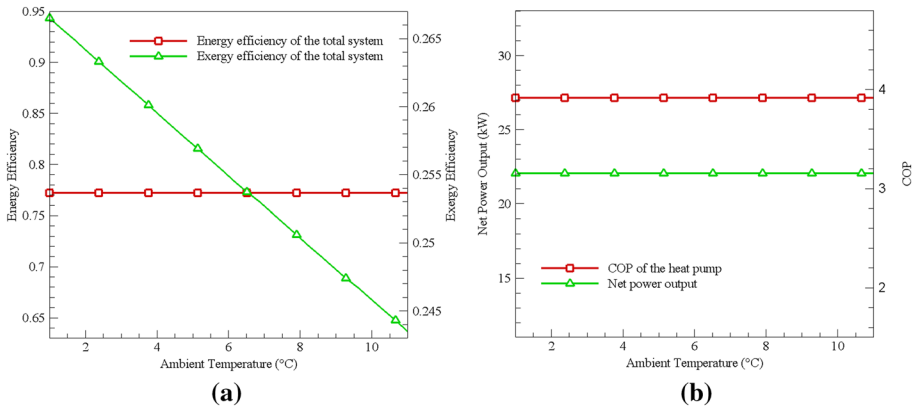

Fig. 10 Effect of ambient temperature changes on **a** energy efficiency and exergy efficiency, **b** net power output and coefficient of performance of the heat pump

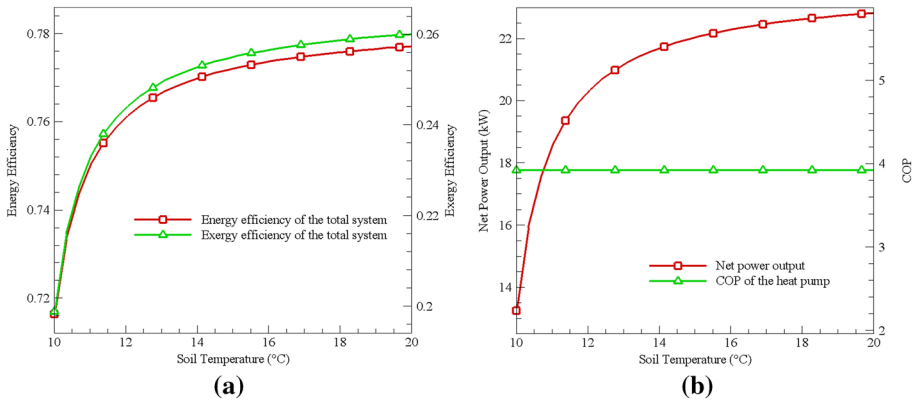

Fig. 11 Effect of soil temperature changes on **a** energy efficiency and exergy efficiency, **b** net power output and coefficient of performance of the heat pump

efficiency, it decreases from 26.65 to 24.35%. Therefore, increasing the ambient temperature will have a negative effect on the system's efficiency. Figure 10b also shows the effects of ambient temperature changes on the total output work and the heat pump performance factor. As the ambient temperature increases from 1 to 11 °C, both system performance parameters remain constant and do not change.

Figure 11a shows the effects of soil temperature changes on energy efficiency and exergy efficiency. As the soil temperature increases from 10 degrees Celsius to 20 degrees Celsius, the energy efficiency of the proposed system increases from 71.64 to 77.71%. In the case of exergy efficiency, it increases from 19.88 to 26%. Therefore, the increase in soil temperature will have a positive effect on the efficiency of the system. The reason for this is the increase in the enthalpy of the geothermal fluid entering the evaporator. Figure 11b also shows the effects of changes in soil temperature on the total output work and the coefficient of performance of the heat pump. As the soil temperature increases from 10 to 20 °C, the net power output of the proposed system increases from 13.24 to 22.83 kW. In the case of the heat pump performance coefficient, it is not affected by soil temperature changes and remains constant at 3.916. As mentioned, the enthalpy increases of the geothermal fluid entering the evaporator.

Hybrid renewable energy systems (HRES) for power generation in remote areas are becoming widespread due to the advancement in renewable energy technology and the price of petroleum products. A hybrid energy system usually uses two or more renewable energy sources that work together to increase system efficiency and balance the energy supply. Geothermal heat is considered a sustainable energy source with significant global potential. A geothermal heat pump can provide clean thermal (cooling) energy for individual and commercial consumers. However, in the conditions of peak electricity demand in the power grid, the need to use an independent and preferably renewable power generation source can be an excellent idea to provide stable and clean electricity for this system. The proposed method investigates how the wind turbine can act as an energy source to supply the required electricity for a geothermal district heating system. The generated electricity is directly transferred to private and commercial consumer units. The results show that wind power can be a suitable complement to a geothermal heat source to provide energy for heating.

Conclusion

In general, a heat pump is a device that transfers energy from the point of origin (low temperature) to the destination point that has a higher temperature. The transfer is done with the help of high thermal energy of the issue with higher temperature or mechanical energy. The difference between the heat pump and conventional air conditioning devices is that the heat pump can transfer heat for cooling and heating. A heat pump can produce cold-like chiller or evaporative systems, which can be done with a cooling cycle (like a refrigerator). In cold regions, heat pumps are used more for heating. Geothermal source heat pumps (GSHP) are central devices that extract heat from deep within the earth and use the earth as a heat source in winter and for heat rejection in summer. This method is one of the optimal heat and cold methods, which is a great help in saving heat and cold costs, which is one of the advantages of this higher productivity system. The general results of the present work are:

- The suggested system's energy efficiency drops from 77.5% to 76.5% by increasing condenser pressure from 1050 to 1550 kPa. Exergy efficiency drops from 25.85% to 24.85%. Increasing condenser pressure reduces system efficiency and, compressor work will boost this. The suggested system's net power production drops from 24.5 to 17.5 kW by increasing condenser pressure from 1050 to 1550 kPa. Heat pump efficiency drops from 4.3 to 3.2. Thus, raising condenser pressure decreases these system performance metrics. This is due to compressors working harder.
- The suggested system's energy efficiency increases from 76.76 to 77.86% by increasing condenser pressure from 153 to 300 kPa. Exergy efficiency rises from 24.4% to 27.21%. Thus, condenser pressure increases system efficiency and, compressor reduction will cause this. The suggested system's net power production improves from 18.8 to 27.18 kW by increasing condenser pressure from 153 to 300 kPa. The heat pump performance factor rises from 3.466 to 4.935. Thus, increasing condenser pressure improves system performance parameters. This is also due to the compressor work decrease.

– The suggested system's energy efficiency increases from 77.19 to 77.22% by increasing condenser pressure from 350 to 500 kPa. 25.46% to 25.55% for exergy efficiency. Thus, condenser pressure increases system efficiency and compressor reduction will cause this. The suggested system's net power production improves from 21.98 to 22.14 kW by increasing condenser pressure from 350 to 500 kPa. The heat pump performance coefficient rises from 3.907 to 3.933. Thus, increasing condenser pressure improves system performance parameters. This is also due to the compressor work decrease. Naturally, mean pressure variations have little effect on these four parameters.

In Shanghai, China, a hybrid system that employs a geothermal heat pump outfitted with an economizer for winter heating and a wind turbine for ecologically friendly power generation was evaluated for its energy and exergy analyses. The hybrid system's processes, as well as every component and the overall design, have been carefully examined. The novel aspect of the current work was the proposal and analysis of the energy and efficiency of a hybrid system that combines a geothermal heat pump with a wind turbine to provide the heat and electricity required for a residential unit in Shanghai, China, during the winter. The research gap on combined heat pump–wind turbine systems is apparent, because so few studies have been conducted thus far.

Acknowledgements
Yashar Aryanfar is receiving a scholarship from the National Council of Science and Technology (CONACYT) of Mexico to pursue his doctoral studies at the Universidad Autonoma de Ciudad Juarez under Grant No. 1162359.

Author contributions
YA: conceptualization, validation, writing original draft, visualization, JLGA: review & editing. The Corresponding author of this manuscript is YA, and the contributions of the authors are confirmed in the research. I would like to take responsibility here by taking the following actions: all authors have been directly involved in the planning, execution, or analysis of this study. Both authors have read and approved the final manuscript.

Funding
Not applicable.

Availability of data and materials
Not applicable.

Declarations

Competing interests
The authors declare thet they have no competing interests.

Received: 19 November 2022 Accepted: 19 March 2023
Published online: 24 April 2023

References

Ahmadi A, Jamali DH, Ehyaei MA, Assad MEH. Energy, exergy, economic and exergoenvironmental analyses of gas and air bottoming cycles for production of electricity and hydrogen with gas reformer. J Clean Prod. 2020;259:120915. https://doi.org/10.1016/j.jclepro.2020.120915.

Allouhi A. Techno-economic and environmental accounting analyses of an innovative power-to-heat concept based on solar PV systems and a geothermal heat pump. Renew Energy. 2022;191:649–61. https://doi.org/10.1016/j.renene.2022.04.001.

Arteconi A, Patteeuw D, Bruninx K, Delarue E, D'haeseleer W, Helsen L. Active demand response with electric heating systems: impact of market penetration. Appl Energy. 2016;177:636–48. https://doi.org/10.1016/j.apenergy.2016.05.146.

Ata S, Kahraman A, Şahin R. Prediction and sensitivity analysis under different performance indices of R1234ze ORC with Taguchi's multi-objective optimization. Case Stud Therm Eng. 2020;22:100785.

Baeten B, Rogiers F, Helsen L. Reduction of heat pump induced peak electricity use and required generation capacity through thermal energy storage and demand response. Appl Energy. 2017;195:184–95. https://doi.org/10.1016/j.apenergy.2017.03.055.

Barton J, Huang S, Infield D, Leach M, Ogunkunle D, Torriti J, Thomson M. The evolution of electricity demand and the role for demand side participation, in buildings and transport. Energy Policy. 2013;52:85–102. https://doi.org/10.1016/j.enpol.2012.08.040.
Bloess A, Schill W-P, Zerrahn A. Power-to-heat for renewable energy integration: a review of technologies, modeling approaches, and flexibility potentials. Appl Energy. 2018;212:1611–26. https://doi.org/10.1016/j.apenergy.2017.12.073.
Connolly D. Heat Roadmap Europe: quantitative comparison between the electricity, heating, and cooling sectors for different European countries. Energy. 2017;139:580–93. https://doi.org/10.1016/j.energy.2017.07.037.
Cooper SJG, Hammond GP, McManus MC, Pudjianto D. Detailed simulation of electrical demands due to nationwide adoption of heat pumps, taking account of renewable generation and mitigation. IET Renew Power Gener. 2016;10(3):380–7. https://doi.org/10.1049/iet-rpg.2015.0127.
Devecioğlu AG, Oruç V. The influence of plate-type heat exchanger on energy efficiency and environmental effects of the air-conditioners using R453A as a substitute for R22. Appl Therm Eng. 2017;112:1364–72.
Dolgun GK, Güler OV, Georgiev AG, Keçebaş A. Experimental investigation of a concentrating bifacial photovoltaic/thermal heat pump system with a triangular trough. Energies. 2023;16(2):649.
El-Shimy M. Optimal site matching of wind turbine generator: case study of the Gulf of Suez region in Egypt. Renew Energy. 2010;35(8):1870–8.
Esen H, Inalli M, Esen M, Pihtili K. Energy and exergy analysis of a ground-coupled heat pump system with two horizontal ground heat exchangers. Build Environ. 2007;42(10):3606–15.
Esposito A. Fluid mechanics with applications. Hoboken: Prentice Hall; 1998.
Fehrenbach D, Merkel E, McKenna R, Karl U, Fichtner W. On the economic potential for electric load management in the German residential heating sector—an optimising energy system model approach. Energy. 2014;71:263–76. https://doi.org/10.1016/j.energy.2014.04.061.
Fuzhang W, Ali S, Nadeem S, Muhammad N, Nofal TA. Numerical analysis for the effects of heat transfer in modified square duct with heated obstacle inside it. Int Commun Heat Mass Transfer. 2021;129:105666.
Gürbüz EY, Güler OV, Keçebaş A. Environmental impact assessment of a real geothermal driven power plant with two-stage ORC using enhanced exergo-environmental analysis. Renew Energy. 2022;185:1110–23. https://doi.org/10.1016/j.renene.2021.12.097.
Hedegaard K, Münster M. Influence of individual heat pumps on wind power integration—energy system investments and operation. Energy Convers Manag. 2013;75:673–84. https://doi.org/10.1016/j.enconman.2013.08.015.
Hepbasli A. Thermodynamic analysis of a ground-source heat pump system for district heating. Int J Energy Res. 2005;29(7):671–87.
Huang X, Ma W, Law C, Luo J, Zhao N. Importance of applying Mixed Generalized Additive Model (MGAM) as a method for assessing the environmental health impacts: ambient temperature and Acute Myocardial Infarction (AMI), among elderly in Shanghai, China. PLoS ONE. 2021;16(8):e0255767.
Huang J, Abed AM, Eldin SM, Aryanfar Y, García Alcaraz JL. Exergy analyses and optimization of a single flash geothermal power plant combined with a trans-critical CO2 cycle using genetic algorithm and Nelder-Mead simplex method. Geotherm Energy. 2023;11(1):4. https://doi.org/10.1186/s40517-023-00247-5.
Jacobson MZ, Delucchi MA, Bauer ZA, Goodman SC, Chapman WE, Cameron MA, Bozonnat C, Chobadi L, Clonts HA, Enevoldsen P. 100% clean and renewable wind, water, and sunlight all-sector energy roadmaps for 139 countries of the world. Joule. 2017;1(1):108–21.
Johnson GL. Wind energy systems. Citeseer: Princeton; 1985.
Kandiri A, Shakor P, Kurda R, Deifalla AF. Modified Artificial neural networks and support vector regression to predict lateral pressure exerted by fresh concrete on formwork. Int J Concr Struct Mater. 2022;16(1):1–22.
Khalil WH. Modeling and performance of a wind turbine. Anbar J Eng Sci. 2007;1:116–30.
Lund JW, Freeston DH, Boyd TL. Direct application of geothermal energy: 2005 worldwide review. Geothermics. 2005;34(6):691–727.
Ma G-Y, Chai Q-H. Characteristics of an improved heat-pump cycle for cold regions. Appl Energy. 2004;77(3):235–47.
Mathew S. Wind energy: fundamentals, resource analysis and economics (Vol. 1). Berlin: Springer; 2006.
Nazar S, Yang J, Ahmad W, Javed MF, Alabduljabbar H, Deifalla AF. Development of the new prediction models for the compressive strength of nanomodified concrete using novel machine learning techniques. Buildings. 2022;12(12):2160.
Ouyang T, Kusiak A, He Y. Modeling wind-turbine power curve: a data partitioning and mining approach. Renew Energy. 2017;102:1–8.
Patteeuw D, Reynders G, Bruninx K, Protopapadaki C, Delarue E, D'haeseleer W, Saelens D, Helsen L. CO2-abatement cost of residential heat pumps with active demand response: demand- and supply-side effects. Appl Energy. 2015;156:490–501. https://doi.org/10.1016/j.apenergy.2015.07.038.
Pishkariahmadabad M, Ayed H, Xia W-F, Aryanfar Y, Almutlaq AM, Bouallegue B. Thermo-economic analysis of working fluids for a ground source heat pump for domestic uses. Case Stud Therm Eng. 2021;27:101330. https://doi.org/10.1016/j.csite.2021.101330.
Quiggin D, Buswell R. The implications of heat electrification on national electrical supply-demand balance under published 2050 energy scenarios. Energy. 2016;98:253–70. https://doi.org/10.1016/j.energy.2015.11.060.
Rodriguez-Alejandro DA, Olivares-Arriaga A, Moctezuma-Hernandez JA, Zaleta-Aguilar A, Alfaro-Ayala JA, Cano-Andrade S. Comprehensive analysis of a vertical ground-source heat pump for residential use in Mexico. Geothermics. 2022;99:102300. https://doi.org/10.1016/j.geothermics.2021.102300.
Ruhnau O, Bannik S, Otten S, Praktiknjo A, Robinius M. Direct or indirect electrification? A review of heat generation and road transport decarbonisation scenarios for Germany 2050. Energy. 2019;166:989–99. https://doi.org/10.1016/j.energy.2018.10.114.
Sanaye S, Niroomand B. Thermal-economic modeling and optimization of vertical ground-coupled heat pump. Energy Convers Manage. 2009;50(4):1136–47.

Sayyaadi H, Amlashi EH, Amidpour M. Multi-objective optimization of a vertical ground source heat pump using evolutionary algorithm. Energy Convers Manage. 2009;50(8):2035–46.
Self S, Rosen M, Reddy B. Energy analysis and comparison of advanced vapor compression heat pump arrangement. The Canadian conference on building simulation. Halifax, Nova Scotia; 2012.
Self S, Reddy B, Rosen M. Ground source heat pumps for heating: parametric energy analysis of a vapor compression cycle utilizing an economizer arrangement. Appl Therm Eng. 2013;52(2):245–54.
Tang X, Yan G, Abed AM, Sharma A, Tag-Eldin E, Aryanfar Y, Alcaraz JLG. Conventional and advanced exergy analysis of a single flash geothermal cycle. Geotherm Energy. 2022;10(1):16. https://doi.org/10.1186/s40517-022-00228-0.
Thiringer T, Linders J. Control by variable rotor speed of a fixed-pitch wind turbine operating in a wide speed range. IEEE Trans Energy Convers. 1993;8(3):520–6.
Ural T, Karaca Dolgun G, Güler OV, Keçebaş A. Performance analysis of a textile based solar assisted air source heat pump with the energy and exergy methodology. Sustain Energy Technol Assess. 2021;47:101534. https://doi.org/10.1016/j.seta.2021.101534.
Waite M, Modi V. Electricity load implications of space heating decarbonization pathways. Joule. 2020;4(2):376–94.
Wang F, Sohail A, Wong W-K, Azim QUA, Farwa S, Sajad M. Artificial intelligence and stochastic optimization algorithms for the chaotic datasets. Fractals. 2022. https://doi.org/10.1142/S0218348X22401752.
Wilson IAG, Rennie AJR, Ding Y, Eames PC, Hall PJ, Kelly NJ. Historical daily gas and electrical energy flows through Great Britain's transmission networks and the decarbonisation of domestic heat. Energy Policy. 2013;61:301–5. https://doi.org/10.1016/j.enpol.2013.05.110.
Zeng C, Yuan Y, Haghighat F, Panchabikesan K, Cao X, Yang L, Leng Z. Thermo-economic analysis of geothermal heat pump system integrated with multi-modular water-phase change material tanks for underground space cooling applications. J Energy Storage. 2022;45:103726. https://doi.org/10.1016/j.est.2021.103726.
Zhai XQ, Yang Y. Experience on the application of a ground source heat pump system in an archives building. Energy Build. 2011;43(11):3263–70. https://doi.org/10.1016/j.enbuild.2011.08.029.

Publisher's Note